Nuclear Instruments and Methods in Physics Research A 335 (1993) 17–29
North-Holland

NUCLEAR INSTRUMENTS & METHODS IN PHYSICS RESEARCH
Section A

Ultra-cold atomic hydrogen beam

W.A. Kaufman, T. Roser [1] and B. Vuaridel [2]
Department of Physics, University of Michigan, Ann Arbor, MI 48109-1120, USA

Received 13 April 1993

We investigated two methods of producing a continuous free beam of electron-spin polarized atomic hydrogen, using a 7.5 T solenoid magnetic field and a helium film-coated cell. The first method involves accumulating H↓ at high field in a 300 mK storage cell and flipping the electron spin by using microwaves to drive a hyperfine transition. The resulting H↑ atoms are accelerated and focused by the solenoid gradient to form an extracted beam. The second method uses the helium film-coated cell as an ultra-cold nozzle. Unpolarized hydrogen is thermalized in high field by collisions with the cell walls; the field gradient subsequently separates the atoms of different spin states to produce an H↑ beam.

1. Introduction

In the past ten years techniques have been developed to create high densities of electron-spin polarized atomic hydrogen [1]. Polarized hydrogen atoms interact via the $^3\Sigma_u$ pair potential. Because this potential supports no bound states, recombination into molecular hydrogen can be very effectively suppressed. A temperature below 0.5 K and a magnetic field larger than approximately 5 T are required to trap and compress the hydrogen atoms. (A field of 5 T corresponds to a spectroscopic energy $\mu B/k_B$ of 3.4 K). Such a trap is often referred to as a magnetic bottle. A common arrangement is to trap the atoms axially with a solenoidal field, and radially with the walls of a helium film-coated cylindrical cell.

The lowest hyperfine energy levels of atomic hydrogen as a function of the external magnetic field are shown in fig. 1. Without external field the four energy levels consist of a singlet state a and the degenerate triplet states b, c and d. A high magnetic field lowers the energy of states a and b and consequently we will refer to these states as "high field seekers" (HFS). Correspondingly, states c and d are called "low field seekers" (LFS). The force acting on the atoms is equal to their effective magnetic moment multiplied by the field gradient. Except at low field (< 507 G) the effective magnetic moments of HFS and LFS are almost equal to the magnetic moment of the electron. The potential energies of LFS and HFS atoms in a solenoidal field are shown in fig. 2.

Without much difficulty, densities of 10^{16} H/cm^3 can be obtained in a magnetic bottle with surfaces coated with superfluid helium. Even higher densities have been reached in studies of atomic hydrogen, but at low hydrogen input flow and in small volumes [2]. For the production of an atomic hydrogen beam of 10^{18} H/s, we estimate that densities of 10^{15} H/cm^3 are sufficient.

We investigated two methods of producing a beam of polarized hydrogen atoms using a magnetic bottle. One method, shown schematically in fig. 2a, consists of storing high densities of HFS atoms and flipping their spins using microwave radiation [3]. If the microwave frequency matches the frequency of either the a to d or b to c transition then LFS atoms are produced at high field. These atoms are accelerated towards low magnetic field and form a beam of atoms in either the d or c state. A second method shown in fig. 2b consists of feeding "warm" atoms into the high field and letting their kinetic energy thermalize by collision with the cold surfaces. Here "warm" refers to atoms having a thermal energy larger than their spectroscopic energy. The LFS atoms are then accelerated towards low magnetic field in a manner similar to the previous method. The HFS atoms are eliminated by recombination into H_2 molecules and subsequent adsorption on a cold surface. We will refer to these methods as the microwave and no-microwave methods, respectively. The no-microwave method is clearly simpler because it does not require a microwave source. It is also possible to

[1] Present address: Brookhaven National Laboratory, Upton, NY 11758, USA.
[2] Present address: Department of Nuclear and Particle Physics, University of Geneva, CH 1211 Geneva 4, Switzerland.

combine these two methods by using microwave radiation with the no-microwave method to convert the HFS atoms into LFS atoms instead of letting them recombine.

Hydrogen atoms with opposite electron spin recombine readily into H_2 molecules; this represents the main limiting factor in achieving high hydrogen throughput. When two atoms recombine they release an energy of 4.48 eV per molecule. Therefore recombination not only leads to a loss of atomic hydrogen but can also cause a large heat load. For example, a hydrogen flow of 10^{18} H/s recombining completely gives rise to a heat load of 358 mW, which is much larger than the cooling power typically available. At a density of about 10^{15} H/cm^3, recombination occurs predominantly on the available surfaces. Clearly the best surfaces to limit recombination are those with low adsorption energies for atomic hydrogen. Teflon is a good candidate and has the additional advantage of being rather free from surface contamination by background gas. Teflon or Teflon-coated surfaces work well from 300 down to 20 K. They have been extensively used in MASER [4] cavities, and also to guide hydrogen atoms from warm dissociators to surfaces at a temperature of about 20 K. At temperatures below 20 K the surface recombination rates become increasingly important. There are no good surfaces known between 20 and 2 K. Frozen molecular hydrogen may be used at about 6 K where the effective recombination rate has a minimum [5]. However, the H_2 coating does not resist the highly corrosive action of the still high recombination rate. At a temperature below 2 K a superfluid helium film is the most suitable surface. The effective

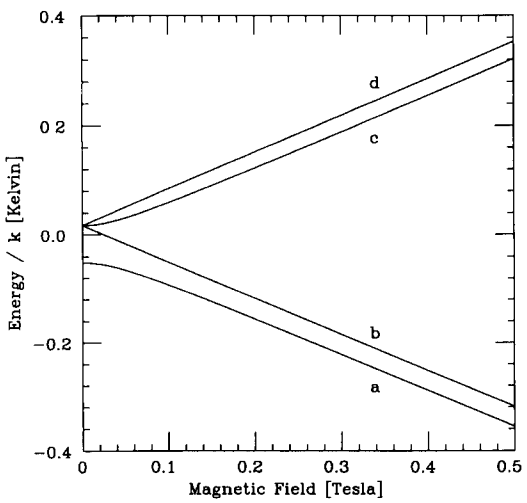

Fig. 1. Energy level diagram of the lowest hydrogen hyperfine states in a magnetic field

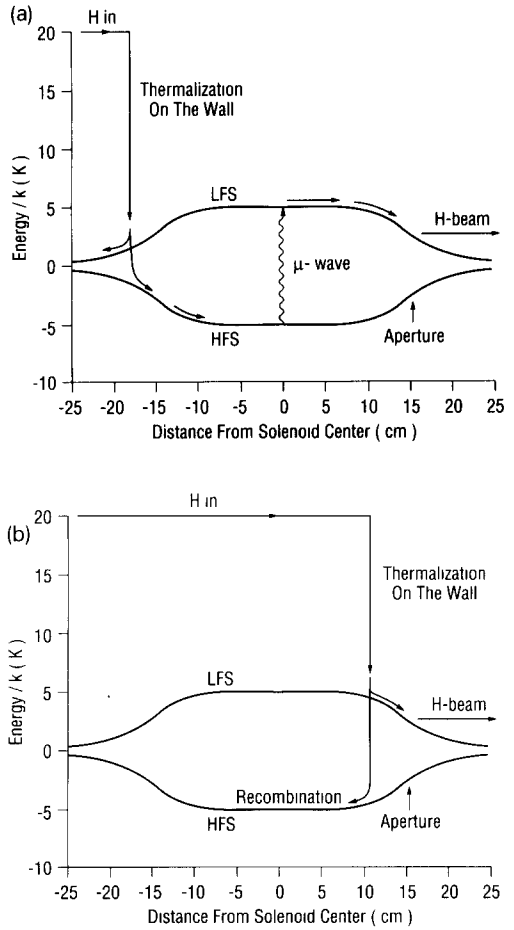

Fig. 2. Potential energy of low field seekers (LFS) and high field seekers (HFS) along the solenoid axis. (a) Atomic hydrogen beam formation using microwave radiation. (b) Beam formation using thermalization in a high field.

volume recombination rate due to surface recombination is given by [6]

$$R = n^2 K^s \frac{A}{V} \Lambda^2(T)\, e^{2\epsilon/k_B T}, \qquad (1)$$

where A is the surface area and V the volume of the cell, Λ is the thermal de Broglie wavelength $(2\pi\hbar^2/Mk_BT)^{1/2}$, k_B is the Boltzmann constant, n is the density, and T is the temperature. The surface recombination rate constant K^s is not strongly dependent on the temperature (see section 6). The adsorption energy ϵ/k_B of atomic hydrogen on superfluid helium film is only about 1 K. The recombination rate is lower at higher temperature; however, a low film temperature is required to keep the helium partial pressure small. Fig. 3 shows the superfluid helium vapor pressure together with its value corrected for molecular transpiration for a room temperature gauge

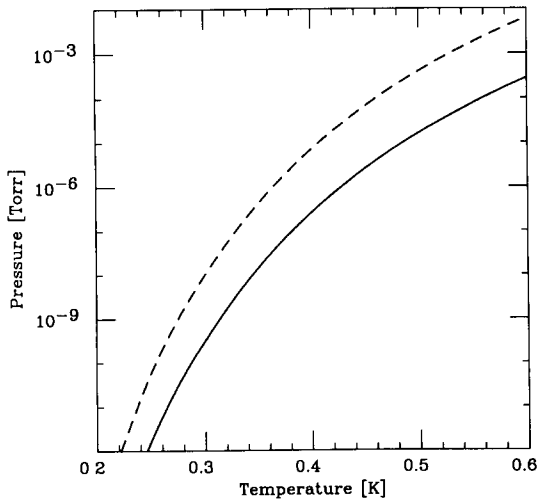

Fig. 3. Superfluid ^{4}He vapor pressure as a function of temperature. The dashed curve is corrected for molecular transpiration for a room temperature gauge.

as a function of temperature. A pressure of 10^{-6} Torr, which is required to avoid excessive beam scattering from the helium background gas, corresponds to a helium film temperature of 350 mK. A temperature between 300 and 350 mK is therefore considered to be a good compromise.

One may consider using either pure ^{3}He or a mixture of ^{3}He and ^{4}He for the film because of the even lower adsorption energy [7,8]. However, the much higher ^{3}He partial pressure then requires an even colder temperature. In fact, the increase in recombination rate due to the lower temperature offsets somewhat the benefit of the lower adsorption energy.

It is worth noting that the adsorption energy for deuterium on helium film [9] is larger than 2 K. In addition, the surface recombination rate K^s at these temperatures is about four orders of magnitude larger [10,11] than for hydrogen, thus increasing considerably the experimental difficulties in producing high deuterium densities in a cell with helium film-coated confining surfaces.

High magnetic fields affect the recombination rate not only by reducing the admixture of electron spin "up" and "down" in states a and c, but also by reducing the overlap of the populations of HFS and LFS in the region where spin selection of the atoms occurs. (We use the term "spin selection" to denote the process of spatially separating the HFS and LFS atoms through use of a magnetic field gradient.) As a general rule the spectroscopic energy should be much larger than the thermal energy. Therefore, for a temperature of about 350 mK the magnetic field has to be larger than 5 T. In addition a high magnetic field improves the focusing of the beam in the fringe field of the solenoid. However, acceleration from a high field results in a higher drift velocity of the beam and consequently lower beam density. The beam density is a maximum when produced in a strong solenoid field gradient (≈ 1 T/cm) at approximately 9 T [12].

Recombination limits the densities that can be achieved with the microwave method. The maximum microwave-driven transition rate is achieved by saturation, which leads to equal LFS and HFS densities. The magnetic bottles we investigated typically have a volume V of 100 cm^3 and a surface area A of 160 cm^2. Using eq. (1), with $\epsilon/k_B = 1$ K, $K^s = 2 \times 10^{-5}$ cm^2/s and $T = 350$ mK, the recombination rate of an equal mixture of HFS and LFS of total density $n = 10^{15}$ H/cm^3 is 8×10^{16} H/s. This corresponds to a heat load of 28 mW, which approximately matches the cooling power of our refrigerator at this temperature. A density of 10^{15} H/cm^3 therefore represents the limiting density of mixed HFS and LFS atoms in our system using the microwave method.

For the no-microwave method, the LFS atoms are accelerated out of the solenoid, while the HFS are pushed toward the center of the solenoid. In principle there are no thermalized atoms which stay in the field gradient. However, the recombination rate for atoms in thermal equilibrium with the cell surfaces does not apply. The effective recombination rate in this case depends on the accommodation and recombination rates of the "warm" 20 K atoms on the cold 300–400 mK surfaces. Unfortunately, to our knowledge neither of these rates have been measured. It is therefore difficult to estimate the limitation of the no-microwave method. For low temperature atoms, accommodation coefficients below 0.2 have been reported [13,14].

A similar situation occurs for the microwave method at the location of the spin selection. In this respect the microwave method is believed to be superior to the no-microwave method because it takes advantage of the full field gradient to accommodate the atoms (see fig. 2), which presumably results in better separation between high and low field seekers.

The maximum magnetic field that can be used with the microwave method is limited by the availability of high frequency microwave sources. At present it is difficult to obtain microwave sources of frequencies much higher than 200 GHz that deliver the required power. This limits the magnetic field to about 8 T.

Naively one would expect that the microwave method would allow the extraction of pure d state atoms which have both full nuclear and electronic spin polarization. However, when the a $\Rightarrow$ d transition is driven the b state atoms are also continuously fed into the magnetic bottle. This density build-up is considerably reduced by the spin exchange reaction b + d $\Rightarrow$ a + c. The large cross-section [3] for this reaction, about 10^{-16} cm^2, is believed to give rise to a spin exchange

rate which, in our apparatus, is larger than the feed rate. Therefore, we expect that the a and b state populations are almost equal in density and the extracted beam consists of an almost equal mixture of c and d state atoms. The situation is then very similar to the no-microwave method.

2. Description of the apparatus

A schematic representation of our apparatus [15] is shown in fig. 4. It consists of a continuous flow high power dilution refrigerator in the vertical section and of an 8 T superconducting solenoid in the horizontal section. The cooling power of the refrigerator is 15 mW at 300 mK. The solenoid has uniformity $\Delta B/B$ better than 10^{-5} over a 10 mm diameter sphere.

The mixing chamber of the dilution refrigerator is a horizontal double-walled copper tube which is located in the 77 mm diameter bore of the solenoid. The space between the two concentric copper tubes forms the mixing chamber, while the inside bore constitutes the storage cell which is fed with hydrogen atoms. We investigated several different mixing chambers. They are presented in section 5.

The hydrogen atoms are produced in a water-cooled

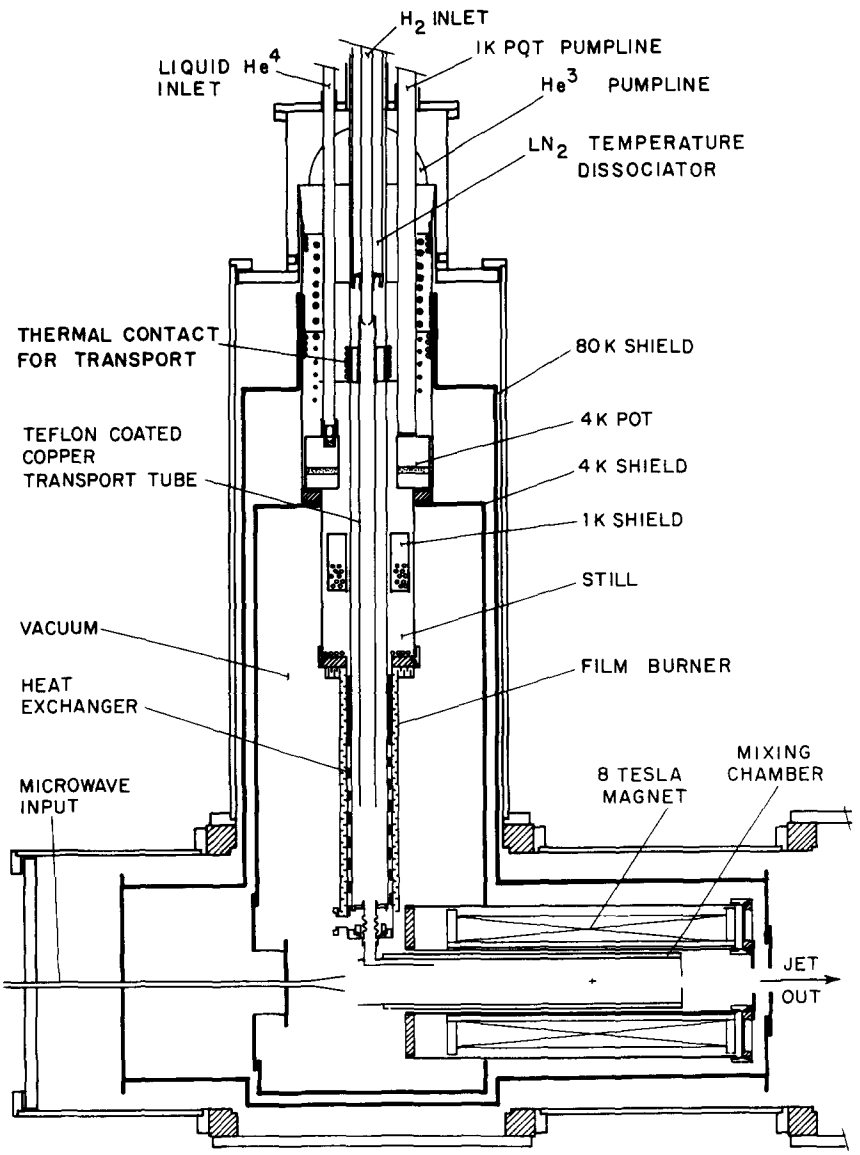

Fig. 4. Schematic diagram of the apparatus showing the vertical dilution refrigerator with the horizontal mixing chamber, the solenoid magnet, and the microwave and hydrogen feed.

room temperature rf dissociator and guided by a Teflon tube to a Teflon-coated copper nozzle operating at a temperature between 20 and 30 K. A fast temperature transition is then made to the mixing chamber which is coated with a superfluid helium film. Details of the feed systems are given in section 4.

The microwave system consists of a 139 to 141 GHz extended interaction oscillator [16]. The microwave frequency stability is better than 5×10^{-5}. The microwave radiation has a power level of 60 mW at the horn, which is shown on the left side in fig. 4. The microwaves are fed into the mixing chamber using the horn, which is cooled to 4.2 K and mounted 20 mm from one end of the storage cell. When baffles are installed in the storage cell, a 4 mm diameter oversized waveguide is used to bypass them. In that case, the diameter of the mouth of the horn is 5 mm, located about 5 mm from the start of the oversized waveguide. We also performed studies at a higher frequency of 213 GHz using a 71 GHz klystron and a microwave tripler [17] operating at 4.2 K. A scalar horn with a 5 mm diameter mouth is mounted directly to the tripler. The output power is 5 mW at the horn. The magnetic field corresponding to this higher microwave frequency is 7.6 T.

The beam which exits towards the right of fig. 4 is detected by a thermal detector, and a sextupole plus compression tube detector. The thermal detector measures the energy released when hydrogen atoms recombine on its bare 4 K copper surface. It consists of three concentric ring detectors made from thin copper foils. All rings have baffles (see fig. 5) to capture a large part of the recombination energy. The rings are thermally linked to a 4.2 K back plane by a brass screw. The energy deposited onto the ring detector is calculated from the temperature increase of the ring. At temperatures between 4 and 10 K the thermal conductivity of brass depends approximately linearly on the temperature. The sensitivity of the detector is therefore temperature dependent. The temperatures of the ring detectors are measured independently with Au + 0.07% Fe–chromel thermocouple junctions. Calibration with electric heaters gave a typical sensitivity of 1 μV emf per μW heating power. The heat signals on the thermal detectors give a lower limit to the actual flow of atomic hydrogen because the "hot" H_2 molecules from recombining atoms do not necessarily deposit all their energy and because some atoms leave the surface before they recombine. In particular, the recombination rate and therefore the signal, depend on the temperature of the detectors. The recombination rate is generally very large at these low temperatures, with a minimum at about 6 K when the surface is coated by frozen hydrogen. Variations of about a factor of two in the signal size were observed by varying the detector temperature while the atom flow was kept constant. All the flows we will quote represent a lower limit, since we always assume 100% detector efficiency. In

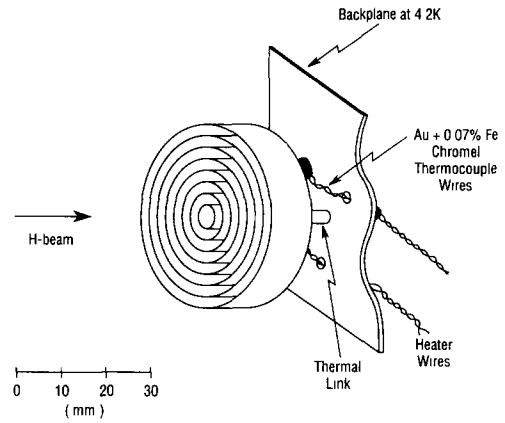

Fig. 5. Thermal recombination detector used for monitoring the atomic hydrogen beam.

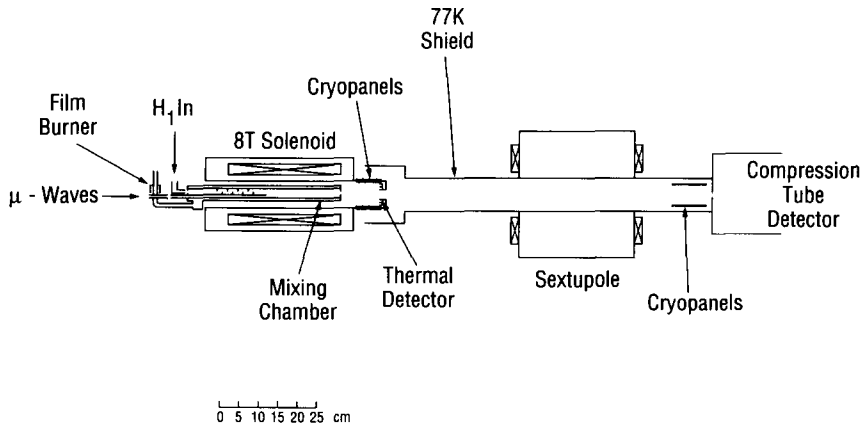

Fig. 6. Lay-out of the beam transport and diagnostics.

the last phase of our investigations the two inner thermal detector rings were removed to allow for the beam to pass through for analysis and detection by the sextupole and compression tube, as shown in fig. 6.

The water-cooled sextupole magnet has a bore of 7.5 cm and a length of 30 cm, with a pole tip field of 3.8 kG at 200 A. This field is high enough to allow for the cold atoms to be focused into the compression tube. A 150 K radiation shield tubing of 6.3 cm diameter inside the sextupole bore reduces the radiation heat load to the mixing chamber and to the cryosorption panels installed along the beam line.

The compression tube detector measures the partial pressure of molecular hydrogen in an enclosed volume whose only openings are a 1 cm diameter hole and a 100 l/s turbomolecular pump. Assuming that all the hydrogen recombines, the molecular hydrogen pressure, as measured by a quadrupole mass spectrometer (QMS) and a cold cathode pressure gauge, is proportional to the flow of atomic hydrogen into the compression tube opening. Both the QMS and pressure gauge were calibrated by bleeding molecular hydrogen into the volume at a measured rate. We always assume that 100% of H atoms recombine into H_2 molecules when we quote a flow measured by the compression tube detector. Such flows are therefore lower limits, as for the thermal detector. We estimate a scale uncertainty of about 20% due to the QMS calibration procedure.

3. Superfluid helium film

All the cold surfaces that come in contact with the atomic hydrogen must be coated with a film of superfluid helium II to avoid rapid recombination. The thickness of this film lies between 1 nm and approximately 50 nm, at which point the film is in equilibrium with the saturated vapor pressure. The pressure has to be kept low to avoid a large heat leak from gas heat exchange with the 4 K heat shield and to avoid scattering of the hydrogen beam from the background helium gas.

Superfluid helium film flows from the coldest towards the warmest surfaces until it evaporates. The helium gas then recondenses at the coldest parts causing a large effective heat leak. The helium pressure is determined by the temperature of the warmest surface that is still coated with helium film. The flow of helium circulating in such a way is approximately given by the flow speed multiplied by its thickness and the width measured transverse to the flow direction. It is thus advantageous to connect the cold mixing chamber with a small diameter tube to the warmer parts of the refrigerator.

To further reduce the helium pressure and to localize the film on the coldest surfaces a device called a

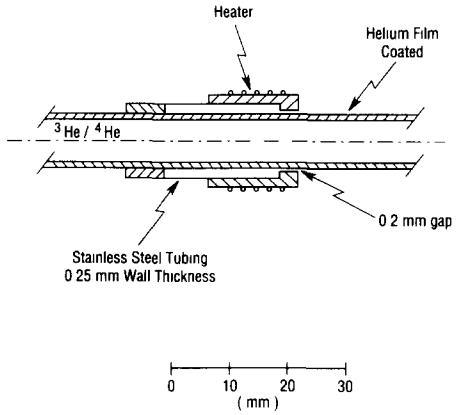

Fig. 7 Schematic diagram of the film burner installed between the helical heat exchanger and the mixing chamber.

"film burner" is used. The film burner consists of an enclosed volume with a small gap towards the film-coated surfaces. Through this gap the film flows into the enclosed volume. To prevent the film from just flowing around the film burner, the outside is thermally isolated from the cold surface and heated with an electric heater. In the inside the film continuously evaporates on the warm surface and recondenses on the cold surface. The helium gas pressure inside can be rather high; however the pressure outside will be much lower due to the low gas conductance of the small gap.

We first investigated a film burner that was installed around the helical heat exchanger as shown in fig. 4. This multistep film burner never worked properly since the temperature at the input was too high. We therefore designed a new film burner as shown in fig. 7. It is located on the tubing connecting the mixing chamber to the helical heat exchanger. Fig. 8 shows the pressure in the vacuum system as a function of the heater power. At low heater power the outside of the film burner is cold and the film creeps around it. At a heater power of about 1 mW the temperature of the outside is between 1 and 2 K and the film burner operates as described above. The pressure in the vacuum system is now drastically reduced. At higher heater power the conduction heat load to the cold tubing becomes increasingly important. The film now evaporates before it reaches the film burner. The minimum pressure we observed here is also the lowest pressure our gauge could read. Thus, the actual helium pressure was probably even lower.

We measured the thickness of the helium film with 1 kΩ resistors suspended on their lead wires at a 5 mm distance from the mixing chamber wall. We supplied 50 μW of electric heating to the resistor and measured the time it took to evaporate the helium as indicated by a drop in its resistance. We obtained an approximate calibration by measuring the total amount of

helium condensed onto the mixing chamber walls and the total outer surface of the mixing chamber. If we assume a film density of about 10^{15} atoms/layer-cm^2, the sensitivity is about 1 layer/ms.

The same resistor can be used to measure the film temperature as long as it is shielded against radiation heat load. For a mixing chamber wall temperature of 200 mK we measured a film temperature of 220 mK. Therefore, the temperature gradient between the film and the mixing chamber walls is negligibly small.

At a somewhat lower temperature the Kapitza boundary resistance may become important. For operation at a lower temperature, or if the film has to be cooled more effectively, a sintered copper surface could be used.

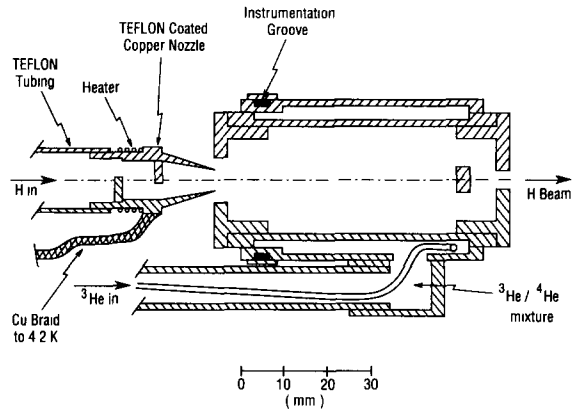

Fig. 9. Schematic diagram of the Teflon-coated copper accommodator and the helium film-coated short cell used for the no-microwave method.

4. Investigation of various feed systems

The room temperature hydrogen atoms are produced in an rf dissociator and are guided into the storage cell by semi-flexible Teflon tubing about 50 cm long and 13 mm in diameter. The atoms are then accommodated to a temperature ranging between 30 and 4 K before they reach the film-coated surfaces.

The transition from the "warm" accommodator to the film-coated surfaces is difficult. For low flux experiments the "warm" surfaces are often in contact with the film-coated surfaces. The film just boils somewhere in between on the thermal break and continuously recondenses onto the film-coated surfaces. As described in the previous section, the film circulates, and the gaseous helium tends to move in the same general direction as the hydrogen atoms. In some cases this effect has been used to compress the hydrogen atoms [18]. Such feed systems work because the heat load due to the recombination on the uncoated surfaces is smaller than the cooling power of the evaporating helium film. The cooling power of the film is typically of the order of 1 mW, depending on its thickness and the length of the boundary that separates film-coated from uncoated surfaces. For fluxes much higher than 10^{15} H/s the film does not provide enough cooling to compensate for the heat of recombining hydrogen atoms on the uncoated surfaces. Therefore, the film will progressively disappear from the whole system when the hydrogen dissociator is switched on.

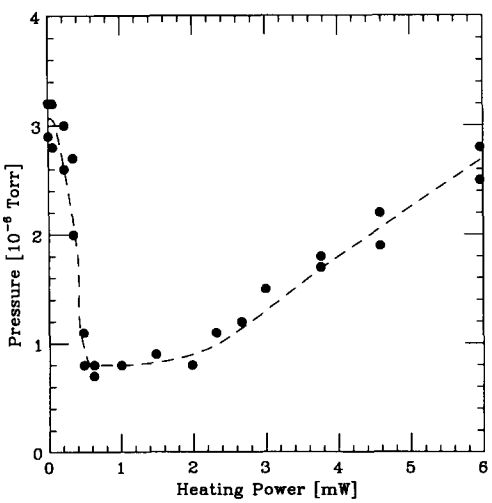

Fig. 8. Insulating vacuum pressure as a function of film burner heating power. The pressure gauge was located at room temperature and calibrated for air.

When a gap separates the film-coated surfaces and the warm accommodator, as shown in fig. 9, the film is stable. However, a large part of the hydrogen atoms are lost because they can escape through this gap. For the system shown in fig. 9, we measured that approximately 10% of the atoms are transmitted through the storage cell, while 90% are lost.

The Teflon-coated copper accommodator shown in fig. 9 gave the best results up to a flow of a few 10^{18} H/s. We typically operated it at about 30 K. For higher fluxes the density of atomic hydrogen in the nozzle is such that recombination becomes increasingly important. It would therefore be necessary to approximately double the size of this accommodator to handle fluxes of more than 10^{19} H/s. In principle, one could also operate the accommodator at a higher temperature, but this would increase the heat load to the film-coated surfaces.

It is tempting to use the film burner concept to design a system with an extremely small gap to reduce the hydrogen losses. We call such an accommodator, shown in fig. 10, a double film burner transition because it has two film burners: one for the inside and one for the outside of the accommodator tube. Note

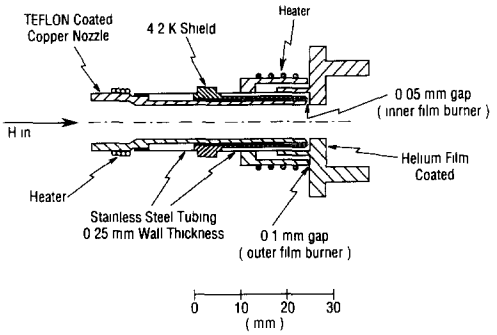

Fig. 10 Schematic diagram of the double film burner transition unit

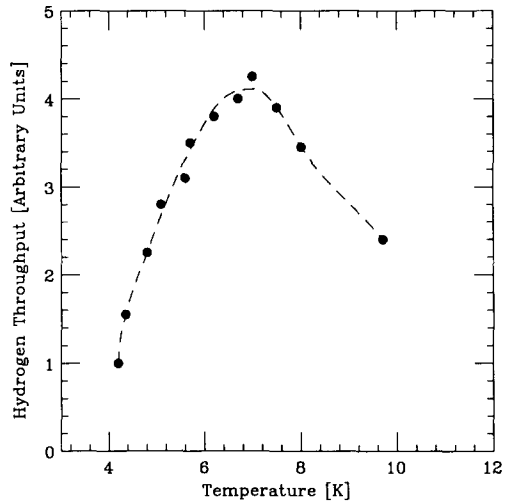

Fig. 11 Hydrogen throughput efficiency as a function of the temperature of a bare copper accommodator

that for a closed cell only the inner film burner would be necessary. The gap of the inner film burner is only about 0.05 mm, to avoid the penetration of hydrogen atoms into the film burner cavity. This system works for a flux of up to 6×10^{16} H/s. However, at a larger flux it is impossible to keep the accommodator at a temperature above the 20 K required for good transmission efficiency, and at the same time retain a stable film. There is probably too much of a heat load to the film close to the accommodator tip.

We also installed a bare copper accommodator operating at 6 K, where the recombination rate of atomic hydrogen on frozen molecular hydrogen is low. This 10 cm long, 13 mm diameter accommodator is cooled with liquid helium and its temperature controlled by a heater. The transmission efficiency of atomic hydrogen through the accommodator versus the temperature is shown in fig. 11. A maximum in the transmission is found at 7 K, in good agreement with earlier measurements [5]. However, the highest transmission efficiency is only about 2%. Furthermore, it was difficult to reproduce the results because of the difficulty in controlling the frozen molecular hydrogen surface. Such an accommodator may be useful for a pulsed atomic hydrogen feed when the averaged flux is low and the frozen hydrogen surface can be recovered between pulses [19].

We can also feed hydrogen atoms through the center of the dilution refrigerator using a 20 K Teflon-coated accommodator 13 mm in diameter. The accommodator is located in the central tubing of the helical heat exchanger as shown in fig. 4. Again it is difficult

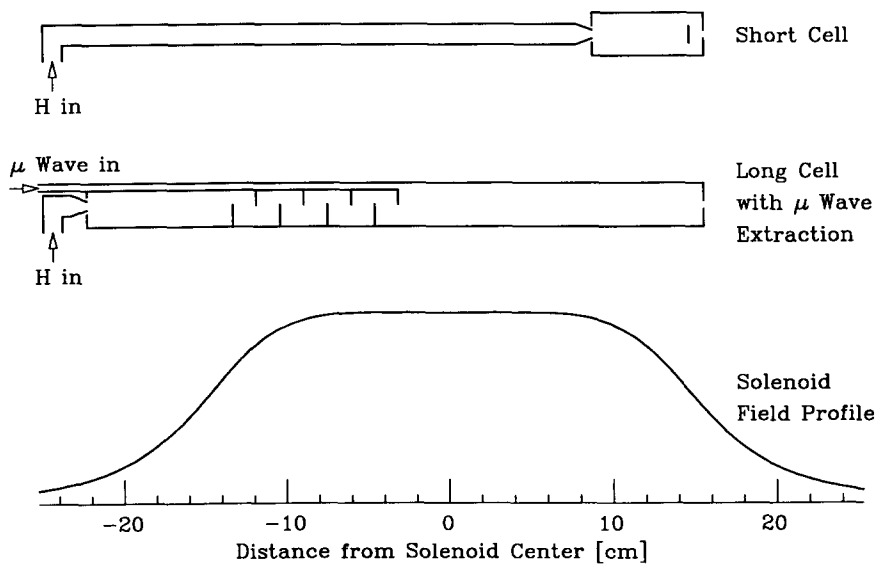

Fig. 12. The long (microwave) and short (no-microwave) cells displayed relative to the solenoid field profile.

to obtain a stable film condition at high fluxes because hydrogen atoms can recombine where the film is boiling. Therefore, the most efficient feed system in our apparatus consists of a 30 K accommodator with a gap between its nozzle and the superfluid film-coated mixing chamber.

5. The storage cells

We have investigated three different cells. Each cell consists of a horizontal double-walled tube made of oxygen-free, high conductivity copper. The space between the two walls forms the mixing chamber of the dilution refrigerator and is filled with the $^3He/^4He$ mixture. All outer surfaces are covered by superfluid helium film. The only essential differences between the cells are their lengths and diameters.

A large cell, 36 cm in length and 4.8 cm in diameter, was used first. It is shown in fig. 4 and was also described in ref. [13]. This cell has a large storage volume of 360 cm^3 where HFS atoms can be accumulated and then extracted using microwave. A detailed description of the measurements performed with this cell can be found in ref. [13]. The large storage volume makes this cell particularly suitable for pulsed operation. The instantaneous pulsed extraction rate was about 10^{16} H/s. The cell is completely open on both sides, and the microwave and the hydrogen atoms are fed from the same side at about 20% of the central field. On the opposite side, the cell ends at about 55% of the central field. With this large diameter and a central field of 5 T, the leakage of HFS atoms is significant, and prevents the buildup of high densities.

A second cell of 36 cm length and 2.5 cm diameter was specifically designed for the production of a continuous beam. It is shown in fig. 12. The hydrogen atoms are fed from the 20 K Teflon-coated nozzle through a 10 mm aperture into the cell. They pass through a system of baffles, to insure that the atoms are well thermalized when they arrive in the central storage volume. An oversized microwave guide bypasses the baffles to feed microwave directly into the storage volume. A flange with a 5 mm aperture on the extraction side reduces the leakage of HFS and forms a low emittance beam of LFS atoms.

The extraction signals, measured by the compression tube as a function of the microwave frequency are shown in fig. 13. The frequency difference between the two extraction maxima is 1.4 GHz, in good agreement with the expected frequency difference between the b ↔ c and a ↔ d transition, which is approximately the zero field hyperfine splitting shown in fig. 1. Note that at 140.54 GHz, which is above the a ↔ d transition frequency corresponding to the maximum magnetic field, no transition can occur. Also, at a frequency

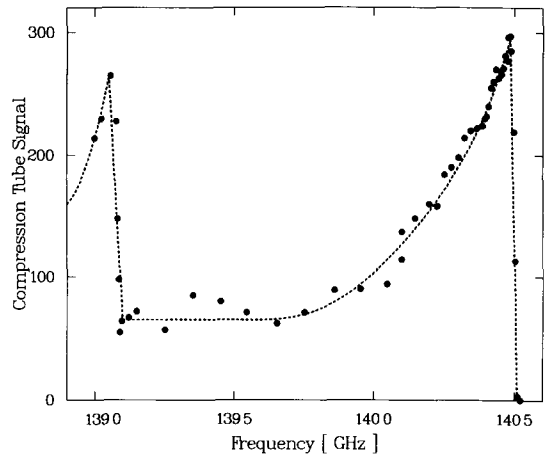

Fig. 13. The compression tube extraction signal measured at a central solenoid field of 5 T, as the microwave frequency was swept through the b ↔ c and a ↔ d transitions.

slightly higher than the b ↔ c transition frequency, a rather high extraction rate is observed. At this frequency, the a ↔ d transition does not take place in the center of the solenoid where the field is the most uniform, but in the field gradient where the field is one percent below its central value. However, correlated with the lower transition probability, we observed an increase in the cell temperature. Presumably, the lower transition probability is partially compensated by a HFS density buildup which leads to increased recombination heat load.

With the microwave frequency properly tuned to one of the transitions, we investigated the focusing property of the beam by the sextupole. The extraction signals measured by the compression tube, and the results of a tracking simulation are shown in fig. 14, as a function of the sextupole current. The focusing is optimum at about 50 A. At higher currents over-focusing reduces the beam flux into the compression tube. For the tracking simulation it is assumed that an equal mixture of c and d state atoms at a temperature of 350 mK effuse from the storage cell aperture, located at 55% of the 5 T central field, are accelerated in the remaining field gradient and are then focused by the sextupole. The simulation predicts a final velocity of 200 ± 20 m/s. An uncertainty in the position of the aperture may cause the location of the tracking calculation peak to shift with respect to the experimental peak. From the good agreement between these curves we can conclude that the extracted beam focused into the compression tube has the expected velocity of about 200 m/s and is highly electron-spin polarized.

The highest continuous flux observed with this storage cell was 1.2×10^{16} (5×10^{15}) H/s onto the outer thermal detector, with a central field of 7.6 (5) T and a

microwave frequency of 213 (140) GHz. The larger flux at 7.6 T/213 GHz was probably obtained because the feed efficiency is better at a higher field. Furthermore, the better spin separation of HFS and LFS should reduce the recombination rates, allowing a higher feed rate. We note that only 5 mW microwave power is available at the tripler horn at 213 GHz. At this low power and high throughput it is especially important to precisely tune the microwave frequency onto a transition (a ↔ d or b ↔ c), otherwise the density in the cell will rise and cause a large recombination heat load. At 5 T/140 GHz, where up to 100 mW microwave power is available, the sensitivity of the system to precise frequency tuning is considerably lower. This suggests that the transition is then almost saturated, i.e. the density of HFS in the cell is at a minimum. Although we estimate that only 10% of the microwave power available at the horn is transmitted to the cell, the actual microwave density inside the cell is enhanced by multiple reflections from the cell walls.

The third cell is only 5 cm long and 2.5 cm in diameter. It is used as a superfluid film-coated nozzle. A schematic representation is shown in figs. 9 and 12. It is possible to move the whole cell so that the exit aperture is located between 40 and 60% of the central field value. The cell entrance aperture is at almost full field, on the same side of the solenoid as the cell exit aperture. This short cell allowed us to test the no-microwave method. The beam fluxes measured by the compression tube versus the current in the focusing sextupole are shown in fig. 15, for various solenoid fields. The curves obtained here were very similar to those of the microwave method, provided the aperture was located at the same position and the central field

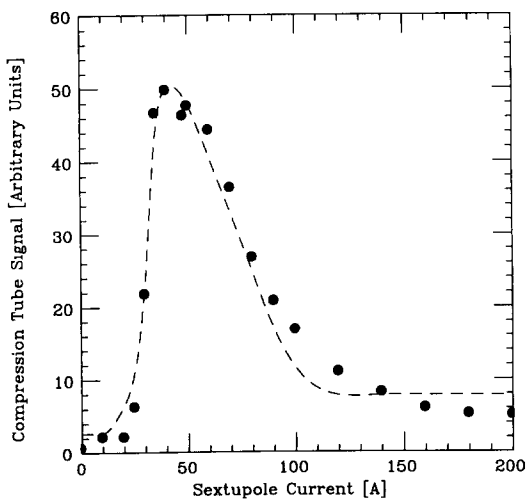

Fig. 14. The compression tube extraction signal at 5 T/140 GHz, as a function of the sextupole current. The dashed curve is the result of a tracking simulation.

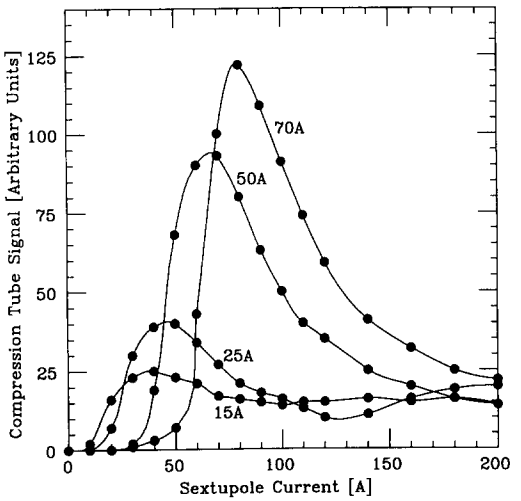

Fig. 15. The compression tube signal as a function of the sextupole current, using the no-microwave method, for several values of the central solenoid field. At 70 A the solenoid field was 7.33 T.

was the same. Clearly, the best performance was obtained at the highest solenoid field with strong sextupole focusing. This is expected due to better feed efficiency as well as a better beam transport at high field. Although we expected the recombination rate to decrease with increasing field because of better spin selection in the cell, no decrease of heat load was observed when the field was raised. Note that the mean velocity of the beam atoms increases with the square root of the solenoidal field resulting in a proportionally reduced beam density. The results of tracking calculations show that a maximum density should be reached when the magnetic field at the exit aperture is about 9 T. At higher fields the gains from the improved focusing properties of the beam are less than the losses in density due to the higher velocity.

For our measurements the field at the aperture was about 3.5 T, about 2.5 times lower than the ideal field value. Under this condition, fluxes up to 3×10^{15} H/s were obtained in the compression tube. The sextupole we used has a small acceptance and only ~ 3% of the extracted atoms reach the compression tube. The system was easy to operate and quite reliable. It seems possible to improve our results by using higher central fields of up to 15 T.

6. Interpretation of the results

It is possible to estimate the densities in the storage cell, the maximum throughput and the recombination rates with simple models. Some ingredients of these models, such as the recombination rates and the ac-

commodation coefficients of atomic hydrogen on superfluid helium are well understood [10]. However, their values were only determined for atoms in thermal equilibrium with the cell walls, which is clearly not the case for 20 K atoms that are accommodated on 300 mK walls. Therefore, rate calculations for the no-microwave cell, as well as for the hydrogen feed side of the larger cells, are more uncertain.

The recombination heat load represents the main limiting factor of our system. It must not exceed the cooling power of the refrigerator, or otherwise the system collapses. The effective volume recombination rate is given by eq. (1); however for polarized atomic hydrogen gas the rate constant K_s depends on the state composition. For example $K_s^{bc} = 4.5 \times 10^{-5}\ T^{1/2}$ cm^2/s for a mixture of b and c states, and $K_s^{ab} = 5 \times 10^{-8}\ T^{1/2}/B^2$ cm^2/s for a and b states, where B is the field in tesla and T is the temperature in kelvin. The recombination rate for a mixture of states i and j with densities n_i and n_j is

$$R = n_i n_j K_s^{ij} \frac{A}{V} \Lambda^2(T)\ e^{2\epsilon/k_B T}. \tag{2}$$

For the microwave method it is possible to model the storage volume, where the atoms are well thermalized after having passed through a set of baffles (see fig. 12). The spin exchange cross section [3] for the reaction b + d $\leftrightarrow$ a + c is about 10^{-16} cm^2. This gives rise to a volume spin exchange rate constant of 8×10^{-13} cm^3/s. This is large in comparison to the volume recombination rate constant at approximately 350 mK, where $K_{ac} \simeq K_{ad} \approx 10^{-15}$ cm^3/s. For a HFS density in the storage cell of about 10^{15} H/cm^3, the spin exchange rate is more than one order of magnitude larger than the feed and extraction rates. Therefore one can assume in our system that the densities of a and b states are almost equal. This is also true for states c and d even if only one transition is driven. Thus, the rate equations can be written in terms of LFS and HFS densities L and H:

$$\begin{aligned} \frac{\partial H}{\partial t} &= \dot{H} \\ &= F - W(H-L) - K_{HL} HL - K_{HH} H^2 - C_H H, \\ \frac{\partial L}{\partial t} &= \dot{L} = W(H-L) - K_{HL} HL - C_L L. \end{aligned} \tag{3}$$

W is the volume transition rate, K_{HL} is the recombination rate constant for a mixture of HFS and LFS, K_{HH} is the recombination rate constant for HFS alone, and C_H is the HFS leakage rate constant. C_H is proportional to $a \exp(\mu_B(B_a - B_c)/k_B T)$, where B_c and B_a are the solenoid fields at the center and the aperture of the cell, and a is the area of the cell aperture. C_L is the conductance for LFS flowing from the center of the cell, where they are produced, to the end of the storage volume, and F is the feed rate. If the microwave is turned on the HFS density H does not build up and the term $K_{HH}H^2$ can be neglected. In an equilibrium situation $\dot{H} = \dot{L} = 0$, and the equation can be easily solved. One of the most interesting results is that increasing the transition rate, i.e. the microwave power, does not lead to an increase in the extraction rate as long as the recombination rate is small. However, at high throughput, high microwave power is necessary to keep the HFS density and thus the recombination heat load low.

Up to this point, the conductance C_L does not take into account the scattering of low field seekers. For a total cross section of 6.5×10^{-16} cm^2 and a LFS density larger than 10^{15} H/cm^3, the mean free path is considerably smaller than the cell diameter. (We have simply used the low energy cross section computed from the s-wave scattering length [20] for LFS. The cross section for scattering of LFS from HFS is considerably smaller.) Using Monte-Carlo techniques one can then compute the effective conductance of the LFS. We find that the effective conductance is given by

$$C_{L_{\text{eff}}}^{-1} = C_L^{-1} + \left(\frac{K}{L}\right)^{-1}, \tag{4}$$

where L is the density of LFS and K is a constant. Also, for a saturated microwave transition $L \simeq H$. Using $C_{L_{\text{eff}}}$ in the rate equations for a saturated transition, the recombination power can be calculated as a function of the feed rate. The results are shown in fig. 16 at 300 and 350 mK for the long 2.5 cm diameter cell. Experimentally we can feed up to about 10^{17} H/s into the storage cell, which corresponds in the model to a

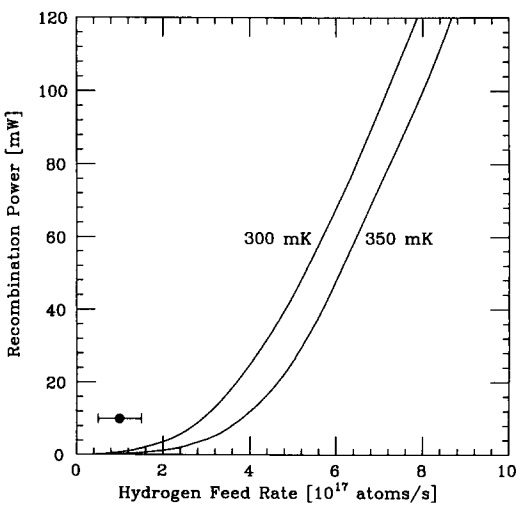

Fig. 16. The recombination heat load versus the hydrogen feed rate for the long (microwave) cell. The curves are based on a simple model described in the text.

negligible recombination power. This was probably the case at 140 GHz, where, with 60 mW of microwave power available at the horn, the microwave transition was close to saturation. The observed heat load is presumably due to heating at the feed side of the cell, which was not included in the modeling.

It was assumed so far that the LFS are free to escape after they have reached the field gradient on the exit side. However, the density of LFS builds up in front of the 5 mm diameter exit aperture, and some overlap between this LFS density profile and that of the HFS exists. This overlap strongly depends on the magnetic field difference between the center and the aperture. However, we found that the recombination heat load did not depend on this field difference, suggesting that this overlap does not cause a significant increase in the recombination.

The feed side of the long cell, and the short no-microwave cell can also be modelled using the following assumption: the atoms are well thermalized after about 30 wall collisions [14], and the average number of wall collisions for an atom before it escapes is much larger than this number. The atoms can then be characterized by the wall temperature. If one neglects at this point the effect of the field gradient on the density profiles, i.e. assumes that the hydrogen inside the cell is unpolarized, the recombination rate per unit volume for the short cell is given by

$$R = 2^{3/2}\pi^{5/2}\frac{A\langle l\rangle\hbar^2\exp(2\epsilon/k_BT)}{Va^2M^{1/2}(k_BT)^{3/2}}E^2, \qquad (5)$$

where M is the mass of the atom, E is the extraction rate, and $\langle l\rangle$, the cross length, is the two dimensional analogue of the cross section. The derivation of eq. (5) assumes effusion from an aperture of area a, and a recombination rate determined by the surface coverage (see eq. (1)). The unpolarized surface recombination rate constant K_s has been eliminated in favor of $\langle l\rangle$ to display the overall dependance on temperature. K_s and $\langle l\rangle$ are related by $K_s = \langle l\rangle v_s$, where $v_s = \sqrt{\pi k_BT/2M}$ is the average velocity in a two dimensional gas. For hydrogen, $\langle l\rangle \simeq 4\times10^{-9}$ cm, $\epsilon/k_B \simeq$ 1K, whereas for deuterium [10,11], $\langle l\rangle \simeq 5.6\times10^{-5}$ cm, $\epsilon/k_B \simeq 2.6$ K. The results for hydrogen are shown in fig. 17 at 300 and 350 mK, together with the heat load observed at maximal hydrogen feed rate. The hydrogen extraction rate E is estimated from the thermal detector signal using tracking simulations that assume effusive flow of a thermalized unpolarized beam from the cell exit aperture. The tracking simulations include the effect of the magnetic field on the atomic trajectories and indicate effective spin separation in the field gradient outside the cell. This extraction rate is probably not very accurate, although good agreement is found between the simple model and the experiment.

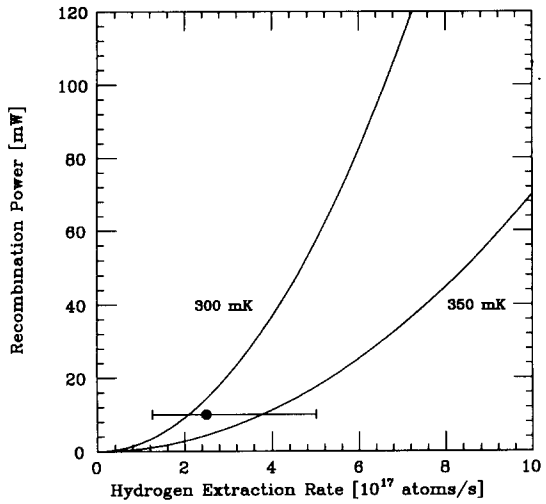

Fig. 17. The recombination heat load versus the hydrogen extraction rate for the short (no-microwave) cell. The curves are given by the simple model described in the text.

We also reproduced, using deuterium, the measured hydrogen heat load on the cell of 10 mW. With this heat load, a temperature of 350 mK, the values for $\langle l\rangle$ and ϵ/k_B given above and the assumption that the atomic deuterium is unpolarized, the density in the cell given by eq. (5) is approximately 4×10^{11} D/cm^3. This corresponds to a total unpolarized effusive flux of 1.2×10^{14} D/s. However, we recorded a thermal detector signal equivalent to an unpolarized effusive flux of approximately 5.7×10^{15} D/s, corresponding to a density in the cell of 1.9×10^{13} D/cm^3, which according to eq. (5) would produce a recombination heat load of about 200 W. This inconsistency can be resolved by assuming that some degree of spin separation does indeed occur for deuterium inside the cell at these lower densities. (The mean free path for polarized deuterium, obtained by using the calculated [21] s-wave scattering length to find the total low energy cross section, is at this density somewhat greater than the cell diameter.) The cross length for polarized deuterium in high field, which is suppressed relative to the unpolarized cross length by a factor $\frac{8}{3}(a_D/3\sqrt{2}\mu B)^2 \simeq 8\times10^{-5}/B^2(T)$, where a_D is the deuterium hyperfine splitting, then comes into play. The observed thermal detector signal would then be consistent with the 10 mW deuterium heat load on the cell.

As mentioned previously, the effect of the field gradient inside the cell on the HFS and LFS, which reduces the density overlap and therefore the recombination rate, has not been considered. In fact, experimentally no significant changes in the heat loads for hydrogen are observed when the solenoid field is var-

ied between 0 and 8 T. This suggests that spin selection of hydrogen is not very effective in the short cell or in the feed side of the long cell, because otherwise it would reduce the overlap of the H and L densities by a factor $\exp(-\mu(B_c - B_a)/kT) \times \mu(B_c - B_a)/(k_B T)$, which is about 100 (10) at 7.5 (5) T, when the aperture is at 55% of the central field. Heat loads from sources other than those in the cell, such as gas exchange between the 20 K nozzle and the film, are proportional to the feed rate. These heat loads are negligible in the case of deuterium because the feed rate was about 50 times lower than for hydrogen. The fact that the experimental results seem to agree with the model indicates that the main heat load is caused by recombination on the film, and that the spin selection for hydrogen is poor.

7. Conclusions

No systematic search has been performed to optimize the cell parameters, and some improvement might be possible. For example, if one doubles all dimensions of the short cell, including the aperture radius, the average number of wall collisions for the thermalization of the atoms, given by the ratio of the inner cell surface area A to the aperture area a, remains the same. The recombination power, however, is proportional to E^2A/a^2. For the same heat load one could then handle about two times the original extraction rate. In principle, one could decrease A, but doing so could reduce the feed efficiency. A different geometry may allow for better spin selection in the gradient, thereby reducing the heat load. With a larger cell and about 100 mW cooling power, it should be possible to feed 10^{19} H/s. A beam of 10^{18} LFS/s could then be produced, given the 10% efficiency of the feed system with a gap. Approximately 30% of such a beam could be focused with a large aperture sextupole onto a 5 mm diameter spot [12]. This would result in a beam density of approximately 2×10^{13} H/cm^2.

Acknowledgements

We wish to thank Professors A.D. Krisch, G.R. Court, T.J. Greytak and D. Kleppner for their support and advice. Drs. D.G. Crabb, V.G. Luppov, Yu.M. Melnick, M. Mertig, A.F. Prudkoglyad, R.S. Raymond, J.A. Stewart, Mr. J.A. Bywater and Mr. P.R. Cameron provided invaluable assistance. The help of Mr. D.P. Stewart and Mr. B.S. Van Guilder was also much appreciated.

This work was supported by a grant from the U.S. Department of Energy.

References

[1] H.F. Hess, D.A. Bell, G.P. Kochanski, D. Kleppner and T. Greytak, Phys. Rev. Lett. 51 (1983) 483;
R. Sprik, J.T.M. Walraven and I.F. Silvera, Phys. Rev. Lett. 51 (1983) 479; 51 (1983) 942;
J.T.M. Walraven and I.F. Silvera, Rev. Sci. Instr. 53 (1982) 140.
[2] T. Tommila, E. Tjukanov, M. Krusius and S. Juakkola, Phys. Rev. B 36 (1987) 6837.
[3] A.P.M. Mattheij, J. van Zwol, J.T.M. Walraven and I.F. Silvera, Phys. Rev. B 37 (1988) 4831.
[4] D. Kleppner, H.C. Berg, S.B. Crampton, N.F. Ramsey, R.F. Vessot, H.E. Petters and J. Vamier, Phys. Rev. A 138 (1965) 972.
[5] R.T. Brackmann and W.L. Fite, J. Chem. Phys. 34 (1961) 1572.
[6] D.A. Bell, H.F. Hess, G.P. Kochanski, S. Buchman, L. Pollack, Y.M. Xiao, D. Kleppner and T.J. Greytak, Phys. Rev. B 34 (1986) 7670.
[7] A.P.M. Matthey, J.T.M. Walraven and I.F. Silvera, Phys. Rev. Lett. 46 (1981) 668.
[8] R. Jochemsen, M. Morrow, A.J. Berlinsky and W.N. Hardy, Phys. Rev. Lett. 47 (1981) 852.
[9] I.F. Silvera and J.T.M. Walraven, Phys. Rev. Lett. 45 (1980) 1268.
[10] I.F. Silvera and J.T.M. Walraven, in Progress in Low Temperature Physics, ed. D F. Brewer (North-Holland, Amsterdam, 1986) vol. X, chap. 3, pp. 139–370, and references therein.
[11] I. Shinkoda, M.W. Reynolds, R.W. Cline and W.N. Hardy, Phys. Rev. Lett. 57 (1986) 1243.
[12] W.A. Kaufman, Nucl. Instr. and Meth. A 330 (1993) 363.
[13] B.W. Statt, Phys. Rev. B 32 (1985) 7160.
[14] J. Helffrich, M.P. Maley, M Krusius and J.C. Wheatley, Phys. Rev. B 34 (1986) 6550.
[15] T. Roser, D.G. Crabb, W.A. Kaufman, R.S. Raymond, J.A. Stewart, B. Vuaridel and G.R. Court, Nucl. Instr. and Meth. A 301 (1991) 42.
[16] Supplied by Varian, Canada.
[17] Supplied by Millitech.
[18] I.F. Silvera and J.T.M. Walraven, Phys. Rev. Lett. 44 (1980) 164.
[19] J.G. Alessi, B. Devito, A. Hershcovitch, A. Kponou, C.R. Meitzler, Proc. 8th Int. Symp. on High Energy Spin Physics, 1988, ed. K.J. Heller, AIP Conf. Proc. No. 187 (1989) p. 1221.
[20] D.G. Friend and R.D. Etters, J. Low Temp. Phys. 39 (1980) 409.
[21] C. Lhuillier, J. Phys. (Paris) 1 (1983) 1.